Geotechnical Testing Journal

doi:10.1520/GTJ20160186 / Vol. 40 / No. 5 / September 2017 / available online at www.astm.org

Huan Wang,[1] Ailan Che,[2] and Shaokong Feng[1]

Quantitative Investigation on Grouting Quality of Immersed Tube Tunnel Foundation Base using Full Waveform Inversion Method

Reference

Wang, H., Che, A., and Feng, S., "Quantitative Investigation on Grouting Quality of Immersed Tube Tunnel Foundation Base using Full Waveform Inversion Method," *Geotechnical Testing Journal*, Vol. 40, No. 5, 2017, pp. 833–845, https://doi.org/10.1520/GTJ20160186. ISSN 0149-6115

ABSTRACT

Full waveform inversion (FWI) method is used to reveal the internal structure of underground mediums in geotechnical engineering. It comprehensively utilizes the amplitude, travel time, and phase of a wave field. It also offers the potential to produce better resolution of the target medium and feasibility for the detection of buried low-velocity layers. A new FWI method for elastic waves in stratified mediums is presented, which adopts a quasi-linear method coupled with a random search algorithm. The strength of this approach is that the Jaccobian matrix is iteratively calculated instead of the Hession matrix, and the inversion work is helpful for getting out of the local minima within appropriate search scope. To verify our method, it is applied to numerical 2-D stratified models and the appropriate search step and range constraint for inversion are determined by parameter sensitivity analysis. With a series of waveform pretreatments, including filter process, waveform energy normalization, and waveforms mitigation based on correlation analysis, we extended it to use with 3-D stratified media models. Its feasibility and accuracy in recovering the unknown parameters of low-velocity layers are certified. Based on the results of the numerical cases, this FWI method can be used for detecting the grouting quality in immersed tube tunnels. The S-wave velocity profiles of low-velocity layers under the tunnel floor are obtained. Because the S-wave velocities of grouting layers will increase before and after grouting, the grouting quality is effectively evaluated by the FWI method and provides a practical reference for other similar projects.

Keywords

full waveform inversion, stratified media, quasi-linearization method, random search, grouting quality

Manuscript received August 4, 2016; accepted for publication March 20, 2017; published online September 8, 2017.

[1] School of Naval Architecture, Ocean and Civil Engineering, Shanghai Jiao Tong University, Shanghai, 200240, China

[2] School of Naval Architecture, Ocean and Civil Engineering, Shanghai Jiao Tong University, 800 Dongchuan-Road, Shanghai, 200240, China (Corresponding author), e-mail: alche@sjtu.edu.cn

Introduction

The study of nondestructive detection for revealing the internal structure of underground mediums has been an important and difficult subject in geotechnical engineering. Many traditional geophysical

methods have been widely used, such as the travel time methods that use the arrival signals of wave components (Ecker et al. 2000; Song et al. 2003), the surface wave methods that involve wave velocity dispersion (Julia et al. 2000; Luo et al. 2007), and the ground penetrating radar methods that are based on the reflection of electromagnetic waves (Matthew et al. 2009; Xu et al. 2010). But the techniques used in some challenging engineering where low-velocity layers are buried, such as the detection of hollowing at the back of tunnel lining, the survey of weak layers underneath strengthening foundations, and the detection for grouted foundation compactness in immersed tube tunnel, have limitations in required quantitative evaluations.

The travel time methods work on the essence of ray tracing and mainly adopt various kinematical characteristics (velocity, distance, time, etc.) to grasp the subsurface medium. These methods have the advantages of little computation and high precision in the high-velocity regions. However, the low-velocity regions are not well characterized by travel time methods. It is reported that refraction tomography is not suitable for the mediums that contain sharp velocity contrast because it reveals this contrast by a gradient zone (Sheehan et al. 2005). Based on the dispersion relationship extracted from seismic synthetic data, the surface wave methods reveal the velocity profile of underground mediums by some inversion algorithms. In the case of shear wave velocity reversals and high stiffness contrasts, the higher modes get more energy and become dominant in frequency dispersion, which is difficult to invert. Also, the information of strata below a low-velocity layer cannot be easily revealed due to a loss of depth sensitivity (O'Neill et al. 2003). Ground-penetrating radar methods interpret the reflected high-frequency electromagnet waves from target mediums and reach the internal dielectric constants by image processing. They are insensitive to other elastic parameters such as elastic modulus and Poisson ratio (Klysz et al. 2004). During the operation, underwater or in the zone with high reinforcement density, the electromagnetic wave shield will greatly restrict application.

At present, the application of the FWI method is gradually promoted in geotechnical engineering for grasping property information carried by response waveforms (Xu 2007). It is available for various elastic parameters of underground mediums by iteratively improving the initial model of the subsurface by matching the observed with modeled data (Plessix 2008; Lefeuve-Mesgouez et al. 2013). It also offers the potential to produce better resolution of target mediums and the feasibility for the detection on buried low-velocity layers. However, the FWI method is a computationally demanding task and still exits obstacles for its full solution, such as the presence of ill-posedness and dependency on the initial model. Many algorithms have been developed to overcome the above obstacles. Sheen et al. (2006) introduced the reciprocity principle and convolution theorem for calculating partial derivatives explicitly, which resulted in a significant decrease of the amount of memory and computation needed for Jacobian and approximate Hessian matrices. Romdhane et al. (2011) performed a FWI algorithm involving both body and surface waves for near-surface investigations with small-scale models.

The framework of the FWI method contains two main critical issues: forward computation and inversion approach. The forward computation is to solve the elastic wave equation and generate accurate response waveforms within underground medium features. Herein, the finite-difference time domain (FDTD) method (Tsingas et al. 1990) is adopted, and the perfectly matched layer (PML) method (Collino 2001; Chen and Bording 2010) is employed as an absorbing boundary condition. The inversion approach is presented in detail in this work. We developed a time-domain FWI algorithm based on the quasi-linearization method, coupled with the random search algorithm (RSA). This algorithm iteratively improves the initial model by systematically fitting it to the observed data. It can be considered as an optimization process that minimizes the misfit between computed response waveforms and observed data, which is usually measured by a least-squares error criterion. Our inversion algorithm is a combination of the non-heuristic and heuristic inversion algorithms (Yamanaka 2005; Virieux and Opertom 2009). It iteratively calculates the Jaccobian matrix for inversion instead of the Hession matrix, improves the initial model by principles of steepest descent, and helps the inversion work get out of the local minima within the appropriate search scope.

The case study is carried out on a 2-D stratified model with three layers to verify our FWI algorithm. It is assumed that the prior information is sufficient and the unknown parameters to be extracted are concentrated on the buried intermediate low-velocity layer. The inversion strategies are determined with parameter sensitivity analyzed by the surface diagram and contour map of objective values. Based on numerical results, we applied it in the site detection for grouting quality in immersed tube tunnels. When the observed data that are acquired from the grouting site, pretreatments including filtering, normalization, and phase adjustment are imposed. Finally, the unknown parameters of the intermediate layer under the tube tunnel are obtained. From the shear wave profiles, the grouting quality is effectively evaluated.

Inversion Method

We combine the quasi-linear method (Fallahi 2012) in time domain with the RSA as is the inversion method in our work. The inversion method is discussed in detail in this section, as well as the terminal conditions and their inversion process.

QUASI-LINEAR METHOD

Assumed that the detection medium is described by a simple model with a limited number of unknown parameters (such as

density, P-wave velocity, and thickness, etc.) to be extracted, the model is described as a parameter vector x,

$$\boldsymbol{x} = (\mathrm{x}_1, \mathrm{x}_2, \ldots, \mathrm{x}_\mathrm{n})^T \tag{1}$$

where subscript numbers denote the unknown parameters in the inversion, respectively, and n is the number of parameters. T denotes the transpose.

As mentioned before, the inversion work is an optimization process that minimizes the misfit between forward computed response waveforms and observed data. This misfit is defined as residual matrix ε:

$$\boldsymbol{\varepsilon}_i = \boldsymbol{F}_i^{\mathrm{obs}} - \boldsymbol{F}_i(\boldsymbol{x}), \tag{2}$$

where $\boldsymbol{F}_i^{\mathrm{obs}}$ and $\boldsymbol{F}_i(\boldsymbol{x})$ are the observed data and the forward computed response waveforms within the model $\boldsymbol{x}$, and indices i denotes the ith receiver. Meanwhile, the objective function Q is introduced as

$$Q = \|\boldsymbol{\varepsilon}\|_2 = \|\boldsymbol{F}^{\mathrm{obs}} - \boldsymbol{F}(\boldsymbol{x})\|_2, \tag{3}$$

where $\|\|_2$ denotes the L2-norm. For a given observed data matrix $\boldsymbol{F}^{\mathrm{obs}}$, there exits an appropriate parameter vector x (global minimum), which makes the forward response waveforms as close as to the observed data as possible. At the start of inversion, an initial parameter vector x^0 is established by prior information and rough estimate. Then, parameter vector x is updated by the quasi-linear method to minimize the misfit as well as the objective function Q, until the global minimum is reached. The parameter vector x in $(\mathrm{n}+1)$th iteration is updated by

$$\boldsymbol{x}^{n+1} = \boldsymbol{x}^n + (\boldsymbol{J} + a\boldsymbol{E})^{-1}\boldsymbol{B}, \tag{4}$$

where E is the identity matrix. J is the Jacobian matrix, which can be obtained by taking the partial derivatives of forward response waveforms with respect to parameter vector x and dot with each other. B is a coefficient vector obtained by partial derivatives of forward response waveforms done with residual matrix:

$$\begin{aligned} J_{p,l} &= \sum_{i=1}^{m}\left(\frac{\partial \boldsymbol{F}_i(\boldsymbol{x})}{\partial x_p}\cdot\frac{\partial \boldsymbol{F}_i(\boldsymbol{x})}{\partial x_l}\right), \\ B_p &= \sum_{i=1}^{m}\left(\frac{\partial \boldsymbol{F}_i(\boldsymbol{x})}{\partial x_p}\cdot\boldsymbol{\varepsilon}_i\right), \quad (p,l = 1,2,3,\ldots,n) \end{aligned} \tag{5}$$

where m is the number of receivers, "·" is the dot operator, and a is Tikhonov regularization parameter (Lampe and Voss 2013) and is determined by Eq 6 in each iteration,

$$\alpha^{k+1} = (1/2)^k T_k^{\max} \tag{6}$$

where k is the iteration time, $T_k^{\max}$ is the maximum eigenvalue of Jacobian matrix $\boldsymbol{J}$ in kth iteration.

Generally, it is difficult to get explicit expression of forward operator F because the derivatives inside Eq 5 are approximately replaced by differential quotient as

$$\frac{\partial \boldsymbol{F}_i(\boldsymbol{x})}{\partial x_p} = \frac{\boldsymbol{F}_i(\boldsymbol{x} + \boldsymbol{\delta x}_p) - \boldsymbol{F}_i(\boldsymbol{x})}{\delta x_p}, \tag{7}$$

where $\boldsymbol{\delta x}_p = (0, \ldots \delta x_p, \ldots 0)^{\mathrm{T}}$. It denotes a slight disturbance on the pth inversed parameter x_p in parameter vector x and this disturbance is taken as 5–10 % of x_p in this work.

As a kind of non-heuristic algorithm, the quasi-linear method has advantages in finite iteration steps, considerable calculate speed, and relatively accurate solutions, but its results and convergence are highly dependent on initial parameter vector x, and can be easily trapped in local minima, which leads to an improbable solution (Fu and Han 2004). So, we adopted RSAs, coupled with the quasi-linear method to mitigate the disadvantages.

RANDOM SEARCH ALGORITHM

RSA is a kind of heuristic algorithm and is derived from the Monte Carlo method (Sambridge and Mosegaard 2002). Based on various search radiuses, a model space was built and the RSA tried stochastic models in it with the purpose of finding a suitable model that decreases the value of objective function Q. Because of its fast speed and global parameter consideration, RSA is very suitable for high-order nonlinear inversion problems with multi-parameter and multiple minima (Huang and Kelka 1996; Kumar et al. 2005).

If parameter vector x output by the quasi-linear method program belongs to the local minimum point, RSA is used to find a new suitable parameter vector, and the new vector x is searched by the following equation (Huang and Kelkar 1995):

$$x_{\mathrm{new},i} = x_{\mathrm{old},i} + (\mathrm{sign}) \times \mathrm{d}x_i \times \mathrm{rand} \tag{8}$$

where $x_{\mathrm{new,i}}$ and $x_{\mathrm{old,i}}$ are the new and unmodified i^{th} parameter respectively, "sign" is search direction and is equal to 1 or −1 with half probability, dx_i is the search radius of each parameter and determined by prior information and empirical estimation, and "Rand" is a random number within the range of [0,1].

The search process will last until the value of objective function Q decreased and the new parameter vector is taken as a new initial parameter vector x of the quasi-linear method. Repeat above steps several times until the terminal condition is satisfied and outputs the last parameter vector as global minimum results.

TERMINAL CONDITION AND STEPS

Two terminal conditions were designed for the iterations of the FWI method. If either of them is satisfied, the calculation is breakout. The first one is related to the objective function. As Eq 7 shows, when the objective function Q is less than a very small

preset value, the difference between observation data G^{obs} and forward data G is considered acceptable.

$$Q^k \leq \eta_1 \tag{9}$$

The second one concerns relative correction. Sometimes, when the iteration is trapped in numerical oscillation, the inversion will breakout. In this state, the terminal condition is shown as below:

$$\sum_{i=k}^{k+c} \frac{Q^i - Q^{i-1}}{cQ^{i-1}} \leq \eta_2. \tag{10}$$

In this work, η_1 and η_2 are preset small values and determined by accuracy requirement of inversion. The superscript k represents kth iteration. The value c represents the fact that the objective function Q keeps stability at least c times during iteration.

The steps of iteration of our FWI method are detailed, as shown in **Fig. 1**.

Numerical Cases

In geotechnical engineering investigation and detection, lots of cases and mediums are simplified as stratified models, so we cast a stratified model with three layers as our numerical case. Meanwhile, the unknown parameters to be extracted were concentrated on the buried intermediate low-velocity layer. At the start, with an assumed known model set of hypocenter and receivers, the response waveforms were obtained by forward computation. Then, this response waveforms data were input into the inversion as if the data were acquired in a field detection as observed data and the underground model is inversed from this observed data. Theoretically, the final results should be the same as the model assumed.

In this section, the case studies are conducted for two purposes. The first is to conclude the inversion rules and protocol from parameter sensitivity analyzed by the surface diagram and contour map of objective values. The second is to verify the ability of our inversion method to reveal features of underground mediums.

TWO-DIMENSIONAL NUMERICAL MODEL

Modeling

As shown in **Fig. 2**, a 2-D stratified model with three layers is established. It is assumed that the material of the first layer is concrete, the third layer is a bearing stratum, and the intermediate layer is a buried weak layer. Their physical property parameters were listed in **Table 1**, where ρ and v_s are the density and S-wave velocity, respectively, h is the thickness, and μ is Poisson's ratio. The PML absorbing boundary is applied on the left, right, and bottom boundary of the numerical model, while the boundary condition on top is set as free. Similar to the field test of hammer sources, the hypocenter is set at upper boundary and a seismic detector is placed 0.5 m away from it. The code in FDTD forward computation consisted of nearly 14,400 nodes spaced 0.05 m vertically and horizontally. Because the maximum P-wave velocity calculated by S-wave velocity and Poisson's ratio in the medium reaches nearly 4,000 m/s, the step of finite difference is taken as 5 μs to satisfy the differential stability conditions. Response waveforms are recorded on the seismic detector; its recorded length is 12 ms (2,400 sampling points). Function of excitation is an artificial signal that covers the most frequency spectrums of various hammer sources. The waveform of artificial signal in time domain and its frequency spectrum within 0.1–4 kHz is shown in **Fig. 3**. The excitation is vertically input on hypocenter and forward computation is carried out. The time-history vertical vibrations on the seismic detector are recorded as response waveforms and considered as observed waveforms $\boldsymbol{F}^{obs}$.

Sensitivity Analysis

The parameters to be revealed are focused on the S-wave velocity v_s and thickness h of the weak layer. To clarify the sensitivities of target parameters to the inversion computation, the thickness h changes from 0.2 m to 2 m with an interval of 0.05 m, while the

FIG. 1
The flow chart of iteration steps of full waveform inversion.

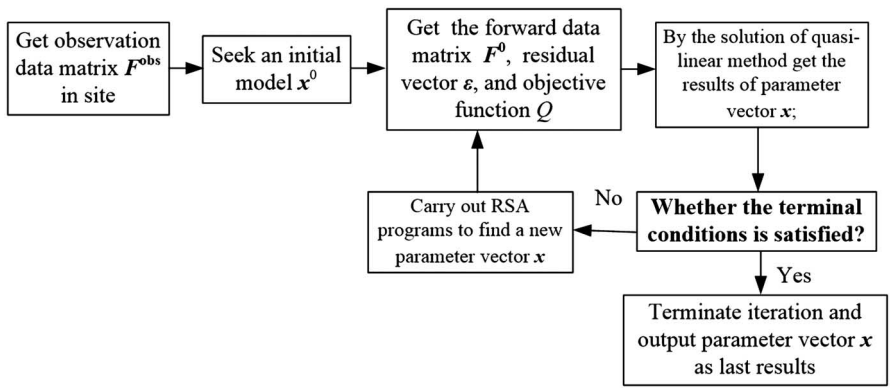

FIG. 2 Two-dimensional stratified model with three layers. (a) Waveform in time domain. (b) Frequency spectrum.

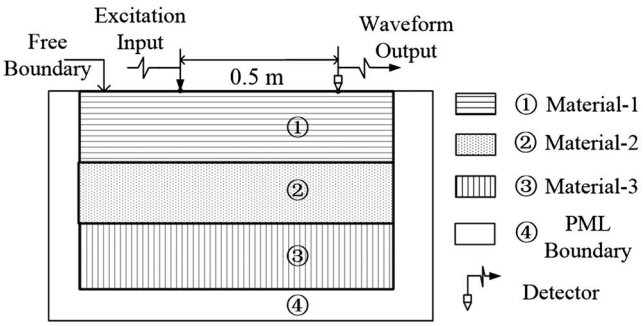

TABLE 1 Material parameters in two-dimensional stratified model.

Layer	Materials	ρ (kg/m^3)	v_s (m/s)	h (m)	μ
Material-1	Concrete	2,400	2,200	1.5	0.18
Material-2	Weak layer	1,800	1,250	0.6	0.3
Material-3	Bearing stratum	2,000	1,800	3.9	0.2

velocity v_s changes from 200 m to 2,000 m with an interval of 25 m. These values of each unknown parameters were combined in order and put into the model for forward computation. As a result, response waveforms under different conditions were calculated, and then the value of objective function is reached, according to Eq 3. All of the results were brought together, and the distribution surface diagram (as **Fig. 4** shows) and contour map (as **Fig. 5** shows) of objective function values that changed with medium parameters were obtained. In **Figs. 4** and **5**, Point A, in which v_s = 1,250 km/s and h = 0.6 m, is the global minimum and the ultimate goal of inversion.

From **Figs. 4** and **5**, it is found that when the wave velocity v_s is lower than 800 m/s, the contour map performs a straight line and large platform in the surface diagram, which indicates that the sensitivities of thickness h is very poor. The decrease of the wave velocity of intermediate layers will cause the reduction of reflection coefficients on the first interface; therefore, little wave energy would penetrate through the intermediate layer, which leads to the poor sensitivities of thickness h. In other words, when the buried low-velocity layers are extremely weak, their wave velocities should be the dominant role in inversion.

As the wave velocity of the intermediate layer increased, the sensitivities of thickness h became increasingly noticeable. There appeared to be many "valleys" near Point A in the surface diagram and many concentric circles in the contour map, which means that many local minimums exit in the zone near global minimum (i.e., Point A), which will affect the global convergence of inversion computation mainly in this zone. To prevent the inversion results from dropping into local minimum and to improve the calculation efficiency, it is advisable to use the appropriate search step for unknown parameters in the inversion (in this work, the search step of inversed v_s is 200 m/s and the thickness h is 0.1 m).

When the intermediate layer reaches high wave velocity or greater thickness, a broad platform appears in the surface diagram and a wide blank area in the contour map. In this zone, the inversion is easily oscillated and aimless. It is strategic to set range constraint on inversed parameters, even if they are obscure (in this work, the inversed v_s is restrained in the range between 800 to 1,600 m/s and the thickness is between 0.2 to 1 m/s).

Inversion Analysis

At the beginning of inversion, the initial inversed parameters in the weak layer are set as h = 0.4 m and v_s = 850 m/s. As the inverse calculation are carried out, the parameters are improved by iterations. Finally, eleven iterations were conducted and the results of the inversed parameters are h = 0.64 m and v_s = 1,250 m/s. The run took about 1.1 s on a laptop computer (2 cores with 2.27 GHz each and 2 GB of memory). Compared with the preset model, the relative errors are 6.7 % and 0 % respectively. The values of objective function for iterations are presented in **Fig. 6**. Also, the final waveforms from the last model with inversed parameters are almost matched with observed waveforms as **Fig. 7** shows.

In addition, in order to clarify the influence of initial inversed parameters on the inversion, five attempts with different initial values were carried out and their final results are listed in

FIG. 3 Hypocenter for observation data in numerical examples.

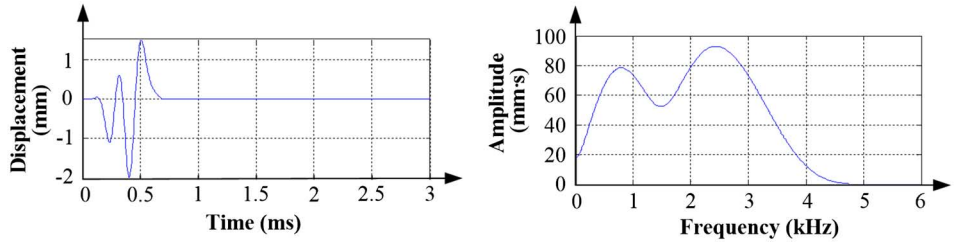

FIG. 4
Distribution surface diagram of objective function values.

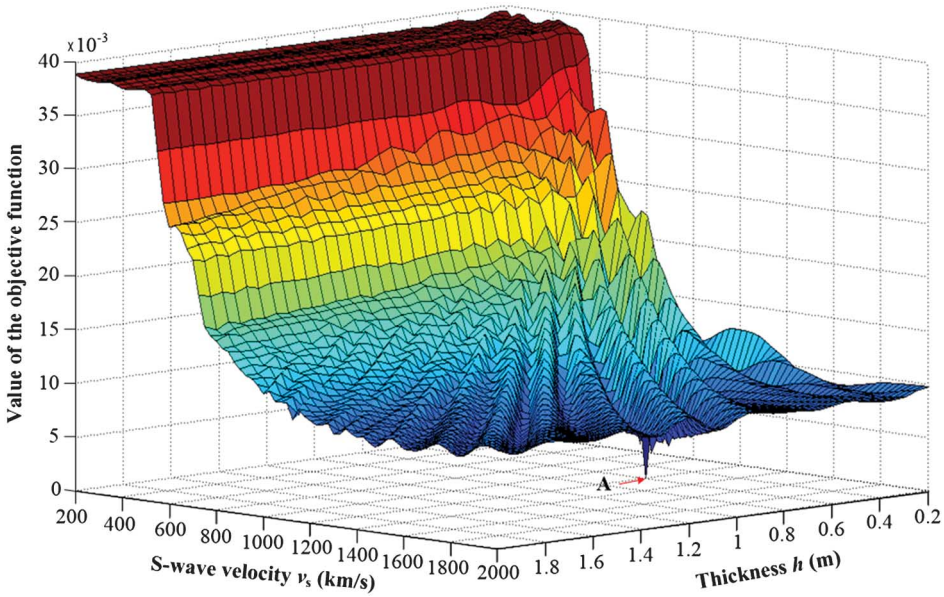

FIG. 5
Distribution contour map of objective function values.

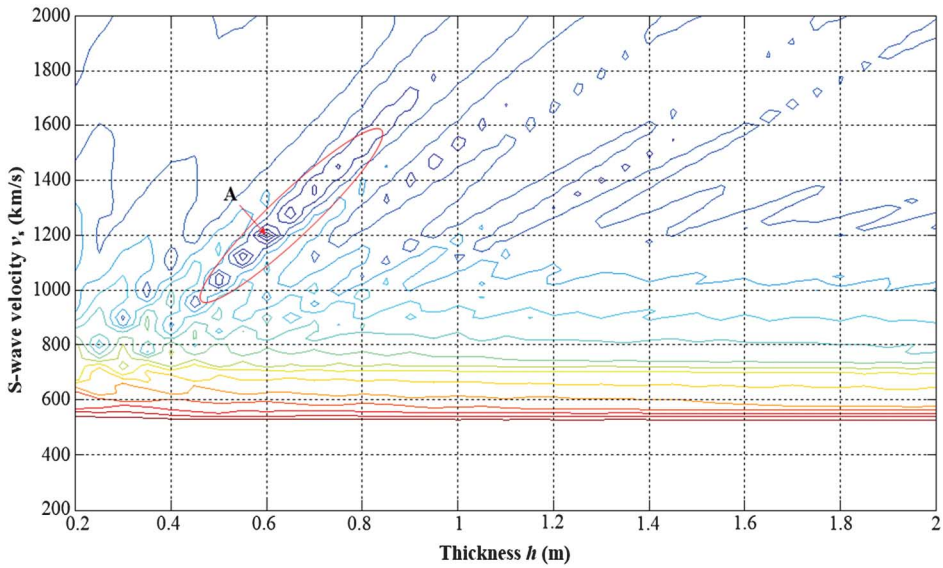

Table 2. In the fourth and fifth attempts, when the initial values of inversed v_s are beyond and exceed the constraint respectively, the computations cost much more with initial values without the constraint. In real cases, the initial values from some other certain information or method are very helpful for the FWI method.

THREE-DIMENSIONAL NUMERICAL MODEL

We extended our FWI method to a 3-D homogeneous stratified model to verify its robustness. However, in most cases, the inversion work is computationally prohibitive because of the large cost of forward calculations of 3-D models, so it was simplified into a 2-D models in inversion work.

Modeling

We cast a 3-D stratified model with three layers as the detection target, as **Fig. 8a** shows, and the extraction was still focused on the intermediate weak layer. Materials and boundary conditions in the 3-D model are the same as the model discussed in "Two-Dimensional Numerical Model," as well as the detection devices. For calculation efficiency, the recorded length is reduced to 6 ms

FIG. 6 Values of objective function and shear wave velocities vary with iterations.

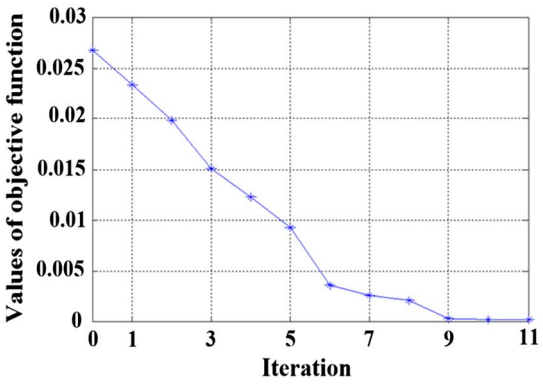

FIG. 7 Comparison between observed and final waveforms of 2-D stratified model. (a) 3-D stratified model. (b) 2-D simplified stratified model.

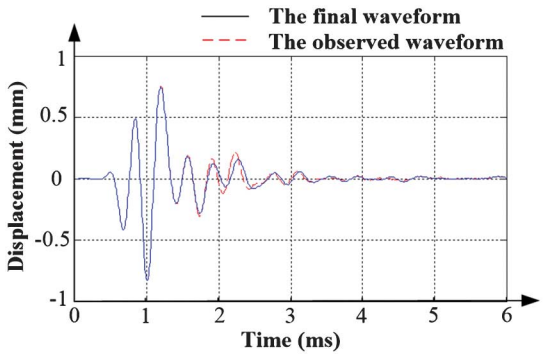

(1,200 sampling points), which is enough for inversion. At the beginning of this numerical example, the forward calculation was carried out on the surface of the 3-D stratified model and the responses waveforms were regarded as observation data.

During the inversion, the simplified 2-D model is used as **Fig. 8b** shows, in which the materials and stratum are the same as those in the 3-D stratified model. Because the propagation of the elastic wave in the 3-D model is spherical and the propagation is fan-shaped in the 2-D model, their wave diffusion and reflection modes are different. As a result, this simplification will cause discrepancy in response waveforms, such as amplitude, frequency, phase, and frequency dispersion. It is reasonable to make the following pretreatments on the forward response waveforms of the 2-D model to smooth the inversion work.

At first, a suitable filter must be loaded on the forward response waveforms to avoid the disturbance of high frequency scattering. Meanwhile, the waveform energy in the low-frequency spectrum is little, which will cause low-resolution in the final results. We adopted a band-pass filter with a spectrum of 300–3,500 Hz in this work.

Secondly, normalization processing based on waveform energy is adopted. The forward response waveforms are attenuated by a coefficient D, which is calculated by Eq 11 in iteration,

$$D = \frac{\int_0^T |\boldsymbol{F}^{\mathrm{obs}}(t)|dt}{\int_0^T |\boldsymbol{F}(t)|dt}, \qquad \boldsymbol{F}^D = D^{-1}\boldsymbol{F}, \tag{11}$$

where T is the length of record time, dt is the sampling interval, and F^{D} is the attenuated response waveform.

Thirdly, to mitigate the discrepancy between frequency spectrums, we translate the attenuated response waveform by a certain distance, which is obtained by signal cross correlation.

According to the definition of cross correlation, the quantification function R_{xy}:

$$R_{xy}(\tau) = \int_{-\infty}^{+\infty} \boldsymbol{x}(t)\boldsymbol{y}(t-\tau)dt \tag{12}$$

where τ is the translated distance, and X and y denote two signals. In order to better characterize the correlation coefficient, we chose the standard deviation of each signal to normalize, and then put the two response waveforms with finite length into the new signal cross correlation, which is reached as Eq 13,

$$R(\tau) = \frac{\int_0^T \boldsymbol{F}^{\mathrm{obs}}(t)\boldsymbol{F}^{\mathrm{D}}(t-\tau)dt}{\sqrt{\int_0^T [\boldsymbol{F}^{\mathrm{obs}}(t)]^2 dt \int_0^T [\boldsymbol{F}^{\mathrm{D}}(t)]^2 dt}}, \tag{13}$$

Table 2 Final results of five attempts with initial values.

No.	Initial Values (h, v_s)	Inversed Results (h, v_s)	Relative Errors	Iteration Times	Time Costs(s)
1	(0.4, 850)	(0.64, 1,252)	(6.7 %, 0 %)	11	1.1
2	(0.8, 1,550)	(0.62, 1,252)	(3.3 %, 0 %)	11	1.1
3	(0.7, 1,400)	(0.6, 1,250)	(0.0 %, 0 %)	12	1.3
4	(0.2, 500)	(0.67, 1,227)	(10.1 %, 1.9 %)	54	58.5
5	(1.2, 2,000)	(0.64, 1,252)	(6.7 %, 0 %)	70	75.8

Notes: The unit of h is m, and the unit of v_s is m/s. The computing works are carried out on a laptop computer (2 cores with 2.27 GHz each and 2 GB of memory).

FIG. 8
3-D stratified model for case study and 2-D simplified stratified model for inversion (the boundary conditions were concealed here).

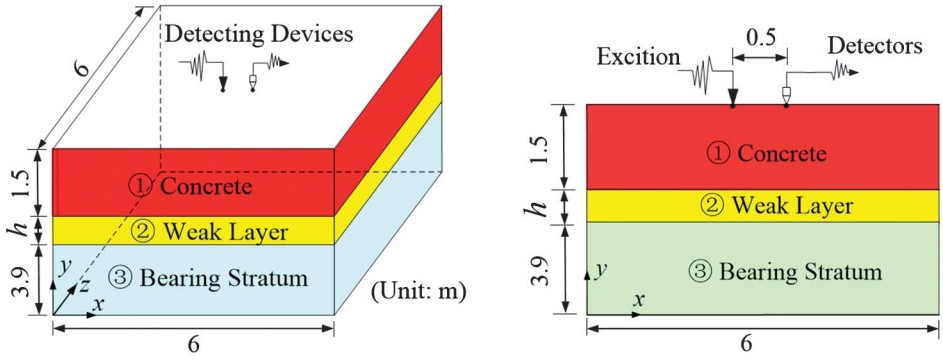

When the coefficient R reaches the maximum, the $\boldsymbol{F}^{obs}$ and $\boldsymbol{F}^{D}$ achieve the most similarity with the translated distance τ. At last, the discrepancies between the two response waveforms are reduced as far as possible.

Inversion Analysis

Similarly to the case study in the section titled "Two-Dimensional Numerical Model," the unknown parameters are thickness h and S-wave velocity v_s of the intermediate weak layer. Processed by the above steps of pretreatments on forward response waveforms of the 2-D model, the inversion computation is carried out. The initial values are given as that h is 0.4 m and v_s is 850 m/s. The objective function values are decreased, along with the iterations as shown in **Fig. 9**; the last results of the parameters are h = 0.68 m and vs = 1,347 m/s.

Because the length of response waveform data is larger than the waveform in numerical example, so the computing time costs more (about 2.3 s on our laptop computer). Compared with the exact values, the relative error of parameters is 13.3 % and 7.8 %, respectively. The final time-domain waveforms agree with the observed, as shown in **Fig. 10**. Different with iterations on conditions of the 2-D model, when the global minimum is reached, the value of objective Q does not approach zero. It is considered a system error between different dimensionalities, but it has less effect on convergence and the accuracy of inversion work. It is concluded that our FWI method and the waveform pretreatments are feasible for the parameters revealed in the 3-D models, and the simplified model with pretreatments have effectively improved the computational efficiency and uncertainty. It makes the FWI method more practical for real cases.

FIG. 9 Values of objective function and shear wave velocities vary with iterations.

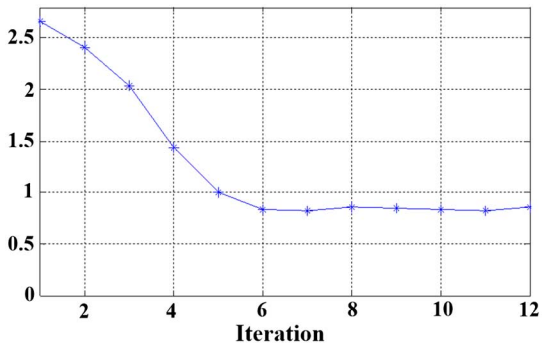

Applications on Field Model Detection

In this section, the FWI method is applied to real data in detection of the grouting quality of immersed tube tunnels. The collected waveform data onsite is pretreated and adopted as observation waveform matrix $\boldsymbol{F}^{obs}$. According to the grouting construction, the model used in the inversion can be simplified as a 2-D stratified model with an intermediate low-velocity layer (grouting layer) buried in it. The thickness and S-wave velocity of the

FIG. 10 Comparison between observed and final waveforms of 3-D stratified model. (a) Measurement line. (b) Hammer. (c) Receiver. (d) Seismograph.

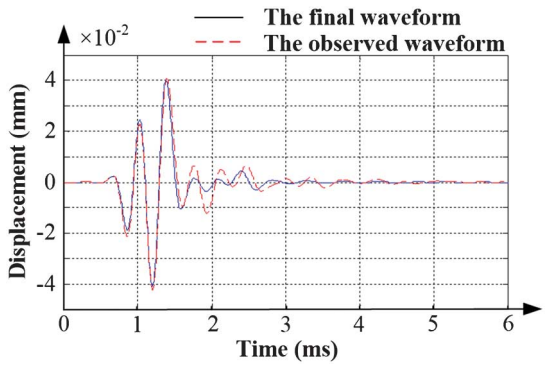

grouting layer are revealed by inverse calculation for the evaluation of grouting quality.

GENERAL

The proposed immersed tube tunnel under Haihe River is located in Yujiabao, the central business district in Tianjin. The immersed tube tunnel is 255 m in designed length, 36.6 m in width, and 9.65 m in height. The thickness of the tube floor is 1.4 m and its strength grade of concrete is C40. In order to satisfy strict seismic resistance requirements and avoid liquidation, traditional sand foundation is replaced by mortar foundation.

Before grouting construction, an intermediate space was preserved between the undersurface of the tunnel floor and the flattened gravel trench, where fulfilled by saturated soil. After grouting construction, the intermediate space was filled with solidified mortar, which became the mortar foundation for the immersed tube tunnel. The high level of grouting quality is important for reducing the uneven settlement of the tunnel and ensuring the safety in daily operations during the service life.

ACQUISITION WORK AND MODELING

The waveform acquisition work onsite was taken three days after the grouting construction. The sketch of the measurement line onsite is shown in **Fig. 11a**. In waveform acquisition work, a round head hammer with a weight of about 680 g was used as hypocenter, as shown in **Fig. 11b**. The receiver, as shown in **Fig. 11c**, was 0.5 m away from the strike point and could detect the vibration signals. A small seismograph, as shown in **Fig. 11d** was applied in order to accept the waveform data from receivers.

Because the various noise vibrations in the work field came from grouting equipment and ship traffic, most of them were in the low frequencies band; the acquired waveform should be filtered by band-pass, whose frequencies were in bands of 300–3,000 Hz. Moreover, it is inevitable that the distance between strike point and receivers could not be kept at 0.5 m perfectly onsite, so the initial phase of the acquired waveform was artificially set to zero to eliminate the influence of phase difference. Besides, as the hammer was manually stroked, the amplitudes of acquired waveforms were not consistent with each other. It is necessary to take energy normalization on the waveforms. Finally, the acquired waveforms were treated as shown in **Fig. 12**.

Based on the design data, experimental results, and construction steps, a stratified initial model with three layers was established by enough prior information. The first layer is concrete and its physical parameters and thickness was obtained from design data. The intermediate layer is saturated soil before grouting and will be replaced by mortar after grouting, and their physical

FIG. 11 Equipment for acquisition work in field (a) before grouting and (b) after grouting.

FIG. 12 Acquired waveforms after the pretreatments (a) before grouting and (b) after grouting.

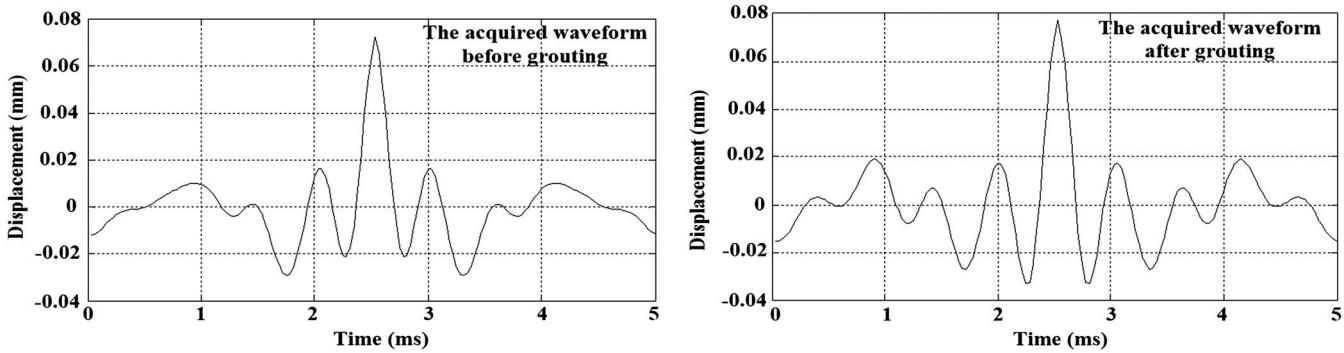

TABLE 3 Material parameters of each layer.

Layers	Material Name	ρ (kg/m^3)	v_s (m/s)	h (m)	μ
1	Concrete	2,500	2,500	1.4	0.18
2-a	Saturated Soil	1,800	inversed	inversed	0.35
2-b	Motor	2,300	inversed	inversed	0.3
3	Gravel & Sludge	2,000	1,500	3.2	0.3

parameters and thickness will be revealed by the FWI method. The third layer is gravel and sludge, its physical parameters and thickness obtained from design data and experimental results. The physical property parameters in the model are listed in **Table 3**.

In the inverse calculation, assumptions and constraints are made as following:

1. All of the materials, except the saturated soil in the model, were assumed isotropic elastic. The boundary conditions are the same as with the 2-D model in "Two-Dimensional Numerical Model."
2. When the intermediate layer was full of saturated soil before grouting, it was strongly inelastic and its S-wave velocity v_s and P-wave velocity v_p could be estimated by empirical formula (Xia et. al 2004) as:

$$v_s = \sqrt{G/\rho}, \qquad v_P = \sqrt{\frac{(\lambda + 2G) + E_w/n}{\rho}} \tag{14}$$

where: E_w is the bulk modulus of water and equal to 2,100 MPa, n is the pore ratio of saturated soil and taken as 0.4 in this work, G is the shear modulus of saturated soil and assumed to be 160 MPa, and λ is the lame constant and taken as 510 MPa.

3. Considering the fact that different combination of discrete stratified models could contribute the same responses, the parameter restriction is adopted to enhance the inversion convergence. Based on the actual conditions of the grouting construction of the immersed tube tunnel, the thickness of the intermediate layer was somewhere between 0.4 and 0.6. Therefore, if the value of thickness was beyond its extent during the iterative calculation, it required corresponding correction.
4. Because most of the energy in the full wave field that was measured on the surface is not sensitive to mass density (Nazarian 1984), the mass density was kept constant during inversion.

WAVEFORM INVERSION BEFORE/AFTER GROUTING

Before grouting, in line with the design and construction schemes, the intermediate layer under the immersed tube tunnel was full of saturated soil with an approximate thickness of 0.5 m. At the beginning of waveform inversion calculation, the initial parameters of the intermediate layer are preset as $h = 0.5$ m and $v_s = 150$ m/s. After many iterations, the results are reached and turn out to be $h = 0.58$ m and $v_s = 221$ m/s. Conversed by Eq 11, the P-wave velocity at this state is 1,753 m/s. The final inversed waveform before grouting is shown in **Fig. 13a**.

After grouting construction, the intermediate soil layer was replaced by a mortar base with a certain degree of solidification. So, before inversion calculation, the initial parameters of the intermediate layer were reset as $h = 0.5$ m and $v_s = 1{,}000$ m/s. Thereafter, calculation was performed with the results of $h = 0.6$ m and $v_s = 1{,}290$ m/s. According to the elastic assumptions, the P-wave velocity at this state was deduced as 2,063 m/s. The final inversed waveform after grouting is shown in **Fig. 13b**.

The above inversion works on a single detection point that reveals the S-wave velocity of the intermediate layer before and after grouting construction, respectively. The S-wave velocity has been highly enhanced from 221 to 1,290 m/s, which means that the grouting quality at the detection point is good.

Similarly, after enough inversion work on each detection point of a measure line was completed, the approximate profiles

FIG. 13 Inversed waveform before/after grouting construction. (a) Before grouting. (b) After grouting.

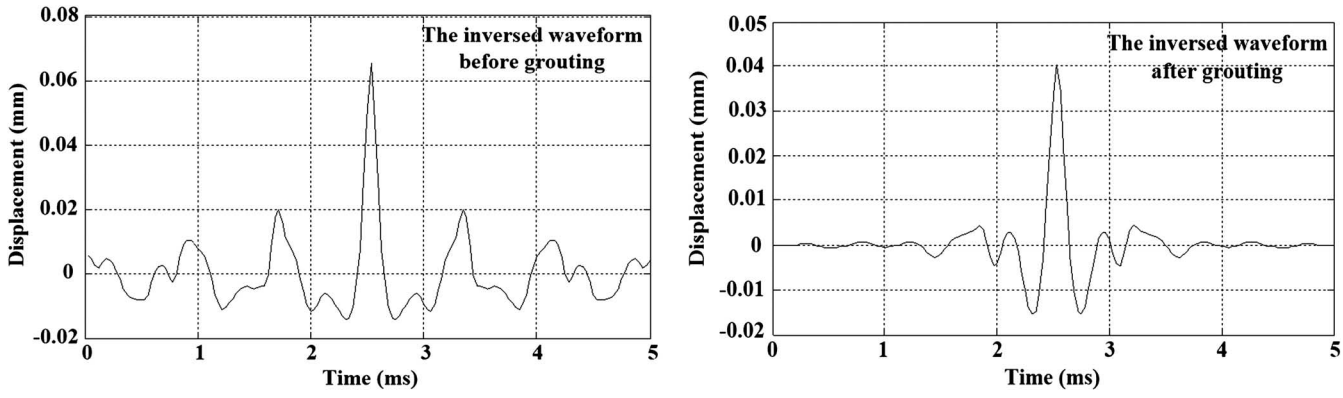

FIG. 14 S-wave velocity profiles from FWI method under a measure line before/after grouting. (a) Before grouting. (b) After grouting.

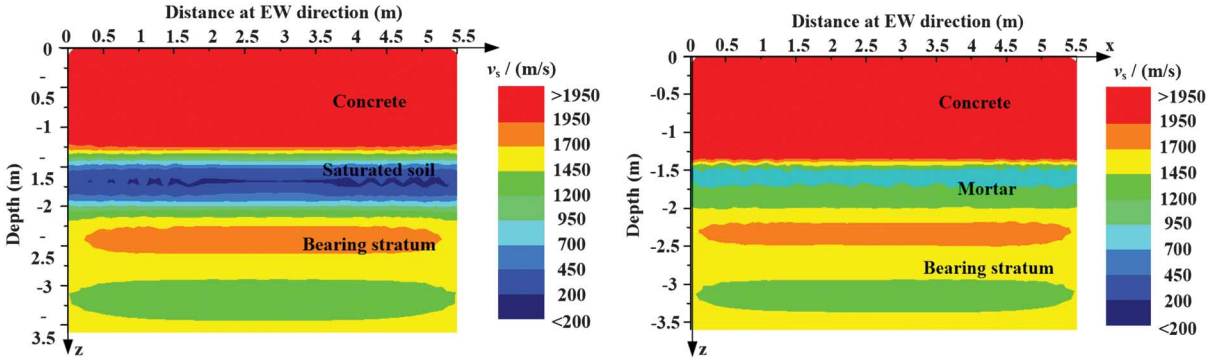

FIG. 15 S-wave velocity profiles from surface wave method under a measure line before/after grouting.

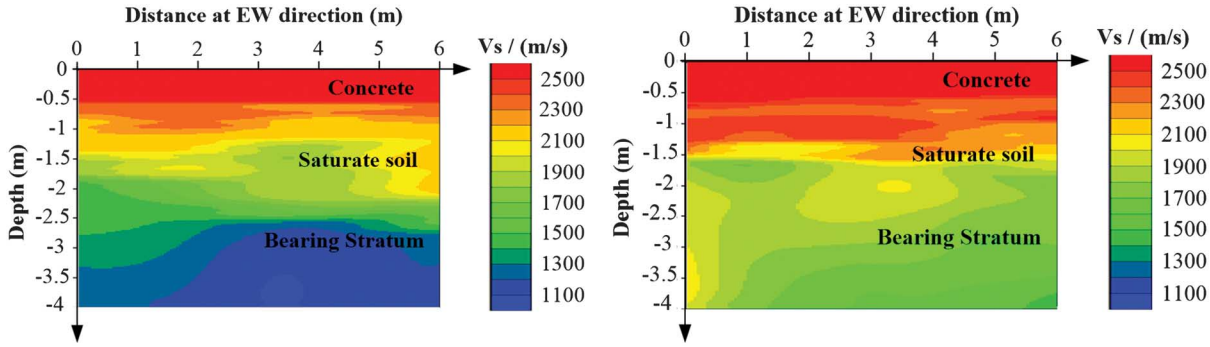

of S-wave velocity under the measure line before and after grouting are achieved, as shown in **Fig. 14**. Compared with S-wave velocity profiles, it was concluded that the grouting quality under the immersed tube tunnel is good. The FWI method is proven to be competent for rapid and effective detection in geotechnical engineering, even real-time monitoring.

For comparison, the S-wave profiles from the surface wave method (see **Fig. 15**) are compared to the profiles from the FWI method (see **Fig. 14**). It is also observed that the FWI S-wave profile appears consistent with the surface wave method on the condition of post-grouting. But, in the condition of pre-grouting, the surface wave method cannot reveal the intermediate low-velocity layer well, whereas the FWI method can feasibly and accurately reach the unknown parameters. Furthermore, because weak layers appear in many ways (caverns, uncompact, and mud mixtures), it is very considerable to make detailed connections between S-wave velocities and weak layers.

Conclusions

A new time-domain FWI method for elastic waves in stratified mediums was developed by adopting a quasi-linear method coupled with RSAs. By quasi-linear method, the Jaccobian matrix is iteratively calculated instead of the Hession matrix and by RSA, the inversion work gets out of the local minima within appropriate search scopes. This FWI method is subsequently tested on both numerical cases and real data. The results from two numerical cases and one real application on an immersed tube tunnel indicated that it is feasible and accurate in revealing the unknown parameters of buried intermediate low-velocity layers.

The appropriate search step and range constraint for inversion are determined by parameter sensitivity analysis. For numerical cases, the unknown parameters low-velocity layer are all well recovered both in 2-D and 3-D models. However, the computations cost much more with initial values without the constraint. When the 3-D model is simplified by the 2-D model in inversion, a series of waveform pretreatments, including filter process, waveform energy normalization, and waveforms mitigation based on correlation analysis, are introduced to ensure successful convergence and suitable computational efficiency. The FWI method was used for detecting the grouting quality in an immersed tube tunnel. From the comparison between profiles of S-wave velocity under the measure line before and after grouting, it was concluded that the grouting quality under the

immersed tube tunnel was good. Also, the FWI method provides a practical reference for other similar projects.

If the detection is required to the extent of all defects, the computer cost enlarges and the inverse convergence declines. As a result, the FWI method is still in need of improvement for better practice.

ACKNOWLEDGMENTS

This work is financially supported by the National Natural Science Foundation of China (No. 11372180).

References

Chen, J. and Bording, R. P., 2010, "Application of the Nearly Perfectly Matched Layer to the Propagation of Low-Frequency Acoustic Waves," *J. Geophys. Eng.*, Vol. 7, No. 3, pp. 277–283, https://doi.org/10.1088/1742-2132/7/3/006

Collino, F. and Tsogka, C., 2001, "Application of the Perfectly Matched Absorbing Layer Model to the Linear Elastic Dynamic Problem in Anisotropic Heterogeneous Media," *Geophys.*, Vol. 66, No. 1, pp. 294–307, https://doi.org/10.1190/1.1444908

Ecker, C., Dvorkin, J., and Nur, A. M., 2000, "Estimating the Amount of Hydrate and Free Gas from Marine Seismic Data," *Geophys.*, Vol. 65, No. 2, pp. 565–572, https://doi.org/10.1190/1.1444752

Fallahi, M., 2012, "The Quasi-Linear Method of Fundamental Solution Applied to Non-Linear Wave Equations," *Eng. Anal. Bound. Elem.*, Vol. 36, No. 8, pp. 1183–1188, https://doi.org/10.1016/j.enganabound.2012.02.016

Fu, H. S. and Han, B. A., 2004, "A Wavelet Multiscale Method for the Inverse Problems of a Two-Dimensional Wave Equation," *Inverse Prob. Sci. Eng.*, Vol. 12, No. 6, pp. 643–656, https://doi.org/10.1080/10682760410001694203

Huang, X. and Kelkar, M., 1995, "Performance Comparison of Heuristic Combinatorial Algorithms for Seismic Inversion," presented at the *65th SEG Annual Meeting*, Houston, TX, *Society of Exploration Geophysicists*, pp. 603–605.

Huang, X. and Kelkar, M., 1996, "Seismic Inversion Using Heuristic Combinatorial Algorithm: a Hybrid Scheme," presented at the *Proceedings of 66th International SEG Annual Conference*, Denver, CO, Society of Exploration Geo-physicists, pp. 1963–1966. https://eurekamag.com/research/019/984/019984828.php

Julia, J., Ammon, C. J., Herrmann, R. B., and Correig, A. M., 2000, "Joint Inversion of Receiver Function and Surface Wave Dispersion Observations," *Geophys. J. Int.*, Vol. 143, No. 1, pp. 99–112, https://doi.org/10.1046/j.1365-246x.2000.00217.x

Klysz, G., Balayssac., J. P., and Laurens, S., 2004, "Spectral Analysis of Radar Surface Waves for Non-Destructive Evaluation of Cover Concrete," *NDT & E Int.*, Vol. 37, No. 3, pp. 221–227, https://doi.org/10.1016/j.ndteint.2003.09.006

Kumar, R., Kabamba, P. T., and Hyland, D. C., 2005, "Analysis and Parameter Selection for an Adaptive Random Search Algorithm," *Math. Comput. Simul.*, Vol. 68, No. 2, pp. 95–103, https://doi.org/10.1016/j.matcom.2004.10.002

Lampe, J. and Voss, H., 2013, "Large-Scale Tikhonov Regularization of Total Least Squares," *J. Comput. Appl. Math.*, Vol. 238, pp. 95–108, https://doi.org/10.1016/j.cam.2012.08.023

Lefeuve-Mesgouez, G., Mesgouez, A., Ogam, E., Scotti, T., and Wirgin, A., 2013, "Retrieval of the Physical Properties of an Anelastic Solid Half Space from Seismic Data," *J. Appl. Geophys.* Vol. 88, pp. 70–82, https://doi.org/10.1016/j.jappgeo.2012.09.010

Luo, Y., Xia, J., Liu, J., Liu, Q., and Xu, S., 2007, "Joint Inversion of High-Frequency Surface Waves with Fundamental and Higher Modes," *J. Appl. Geophs.*, Vol. 62, No. 4, pp. 375–384, https://doi.org/10.1016/j.jappgeo.2007.02.004

Matthew, R. B., Nigel, J. C., and Jeremy, P., 2009, "Internal Structure of a Barrier Beach as Revealed by Ground Penetrating Radar (GPR): Chesil Beach, UK," *Geomorphology*, Vol. 104, Nos. 3–4, pp. 218–229, https://doi.org/10.1016/j.geomorph.2008.08.015

Nazarian, S., 1984, "In Situ Determination of Elastic Moduli of Soil Deposits and Pavement Systems by Spectral-Analysis-of-Surface-Waves Method," Ph.D dissertation, The University of Texas at Austin, Austin, TX.

O'Neill, A., Dentith, M., and List, R., 2003, "Full-Waveform P-SV Reflectivity Inversion of Surface Waves for Shallow Engineering Applications," *Explor. Geophys.*, Vol. 34, No. 3, pp. 158–173, https://doi.org/10.1071/EG03158

Plessix, R. E., 2008, "Introduction: Towards a Full Waveform Inversion," *Geophys. Prospect.*, Vol. 56, No. 6, pp. 761–763, https://doi.org/10.1111/gpr.2008.56.issue-6

Romdhane, A., Grandjean, G., Brossier, R., Rejiba, F., Operto, S., and Virieux, J., 2011, "Shallow-Structure Characterization by 2D Elastic Full-Waveform Inversion," *Geophysics*, Vol. 76, No. 3, pp. 81–93.

Sambridge, M. and Mosegaard, K., 2002, "Monte Carlo Methods in Geophysical Inverse Problems," *Rev. Geophys.*, Vol. 40, No. 3, pp. 3-1–3-29.

Sheen, D. H., Tuncay, K., Bag, C. E., and Ortoleva, P. J., 2006, "Time Domain Gauss-Newton Seismic Waveform Inversion in Elastic Media," *Geophys. J. Int.*, Vol. 167, No. 3, pp. 1373–1384, https://doi.org/10.1111/gji.2006.167.issue-3

Sheehan, J. R., Doll, W. E., and Mandell, W. A., 2006, "An Evaluation of Method Sand Available Software for Seismic Refraction Tomography Analysis," *J. Environ. Eng. Geophys.*, Vol. 10, No. 1, pp. 21–34, https://doi.org/10.2113/JEEG10.1.21

Song, H. B., Matsubayashi, O., and Kuramoto, S., 2003, "Full Waveform Inversion of Gas Hydrate-Related Bottom Simulating Reflector," *Chin. J. Geophys.*, Vol. 46, No. 1, pp. 44–52, https://onlinelibrary.wiley.com/doi/10.1002/cjg2.315/full

Tsingas, C., Vafidis, A., and Kanasewich, E. R., 1990, "Elastic Wave Propagation in Transversely Isotropic Media Using Finite Differences," *Geophys. Prospect.*, Vol. 38, No. 8, pp. 933–949, https://doi.org/10.1111/gpr.1990.38.issue-8

Virieux, J. and Operto, S., 2009, "An Overview of Full-Waveform Inversion in Exploration Geophysics," *Geophys.*, Vol. 74, No. 6, pp. 1–26. https://en.cnki.com.cn/Journal_en/C-C037-SLXB-2004-11.htm

Xia, T. D., Yan, K. Z., and Sun, M. Y., 2004, "Propagation of Rayleigh Wave in Saturated Soil Layer (in Chinese)," *J. Hydraul. Eng.*, Vol. 11, pp. 81–84.

Xu, X., Zeng, Q., Li, D., Wu, J., Wu, X., and Shen, J., 2010, "GPR Detection of Several Common Subsurface Voids Inside Dikes

and Dams," *Eng. Geol.*, Vol. 111, Nos. 1–4, pp. 31–42, https://doi.org/10.1016/j.enggeo.2009.12.001

Xu, N., 2007, "Seismic Characteristics of Gas Hydrates in East China Sea and Study of Full Waveform Inversion," Ph.D dissertation, Institute of Oceanology, Chinese Academy of Sciences, Qingdao, China.

Yamanaka, H., 2006, "Comparison of Performance of Heuristic Search Methods for Phase Velocity Inversion in Shallow Surface Wave Method," *J. Environ. Eng. Geophys.*, Vol. 10, No. 2, pp. 163–173, https://doi.org/10.2113/JEEG10.2.163